



HAL
open science

Non-lithostatic pressure in subduction zones

Hugues Raimbourg, Gaku Kimura

► **To cite this version:**

Hugues Raimbourg, Gaku Kimura. Non-lithostatic pressure in subduction zones. *Earth and Planetary Science Letters*, 2008, 274 (3-4), pp.414-422. 10.1016/j.epsl.2008.07.037 . insu-00756073

HAL Id: insu-00756073

<https://insu.hal.science/insu-00756073>

Submitted on 22 Nov 2012

HAL is a multi-disciplinary open access archive for the deposit and dissemination of scientific research documents, whether they are published or not. The documents may come from teaching and research institutions in France or abroad, or from public or private research centers.

L'archive ouverte pluridisciplinaire **HAL**, est destinée au dépôt et à la diffusion de documents scientifiques de niveau recherche, publiés ou non, émanant des établissements d'enseignement et de recherche français ou étrangers, des laboratoires publics ou privés.

Non-lithostatic pressure in subduction zones

Hugues RAIMBOURG

IFREE, JAMSTEC, Yokosuka, Japan

Gaku KIMURA

Dpt. Earth and Planetary Science, The University of Tokyo, Japan

Abstract

The pressure at depth is not directly observable and no one knows precisely to which extent the pressure conditions in subduction zones, recorded by high-pressure metamorphic rocks, deviate from mantle lithostatic pressure. As an alternative to large-scale complex numerical models of subduction zones, the analytical subduction channel model can give us some insight on the physical processes that control the development of non-lithostatic pressure, as well as some estimation of its amplitude. We propose a new approach coupling the flow of crust within the channel to the deformation of the mantle bounding the channel, occurring as the pressure within the channel deviates from mantle lithostatic values. While for very weak crust within the subduction channel, the channel walls are rigid and channel geometry does not vary, for stronger crust, our coupled approach unravels a new domain of behaviour where the mantle is no longer completely rigid and the deformation of the channel walls prevents arbitrarily large non-lithostatic pressure to develop. This new regime poses an upper bound on the amplitude of non-lithostatic pressure within the channel that depends only on the mantle viscosity. The transition from one regime to another is dependent on an adimensional parameter $\alpha = \frac{\mu_m}{\mu_c} \frac{h_0^3}{L^3}$, incorporating not only mantle and crust viscosity but also the geometry of the channel. The development of larger non-lithostatic pressure

in thinner channels than in larger ones, predicted in the rigid channel model, is partly inhibited in the fully coupled model as thinner channels more easily induce channel wall deformation. The lengthscale of the channel width perturbations influences the amplitude of non-lithostatic pressure, as small-scale ones, inducing a more rigid response of the mantle, potentially trigger larger non-lithostatic pressure.

1 Introduction

Petrological analysis of metamorphic rocks is a powerful tool to assess the circulation of crustal material, as it enables to decipher P T conditions recorded by a given rock during its evolution. In order to build geodynamical models, P is commonly converted into depth assuming a mantle lithostatic pressure gradient. This assumption has been challenged in analytical and numerical models (Mancktelow, 1993; Mancktelow, 1995; Mancktelow, 2007; Petrini and Podladchikov, 2000) as well as in geological and petrological studies (Duchêne and Ford, 2006; Stüwe and Sandiford, 1994), leading to the much controversial concept of non-lithostatic pressure (i.e. deviations from the mantle lithostatic pressure).

The doubt cast by such studies is most acute in subduction zones, where extremely large pressures are recorded by deeply buried rocks (Chopin, 1984; Smith, 1984). Numerical models of subduction zones are numerous, but they give somehow disagreeing results as

regards the extent of non-lithostatic pressure, predicting either under- (Toussaint et al., 2004), overpressure (Burg and Gerya, 2005), or neglectible non-lithostatic pressure (Burov et al., 2001). In addition, because of their complexity itself, such studies cannot provide any explicit relationship between the extent of non-lithostatic pressure and other relevant parameters.

The analytical “subduction channel” model (England and Holland, 1979; Shreve and Cloos, 1986) is the appropriate tool to describe circulation of the thin layer of crust on top of the slab and to decipher the physical processes controlling the associated pressure field. This subduction channel was the framework chosen by (Mancktelow, 1995) to derive extremely large (1GPa) overpressures, equivalent to the pressure generated by a 30km-thick rock column.

We propose here first to briefly describe why the question of the amplitude of non-lithostatic pressure is a relevant one and then to reassess such non-lithostatic pressure and the general flow properties within the subduction channel, using a new approach coupling both crustal deformation within the channel and deformation of the channel geometry itself.

2 Review of the non-lithostatic pressure concept in subduction zones

The first process through which non-lithostatic pressure may be generated within

subduction zones, proposed by Jischke (Ref??), is related to the global force balance:

The non-lithostatic pressure concept is rather unpopular, as many geologists believe either that non-lithostatic pressure, i.e. deviations from the mantle lithostatic pressure, are of sufficiently limited amplitude, or that they are only a transient phenomenon that vanishes sufficiently quickly to be disregarded. Before developing our analysis, it seems therefore necessary to precise what kind of mechanisms may possibly trigger the development of persistent non-lithostatic pressure in the deformed zone on top of the slab.

2.1 Non-lithostatic pressure as a force balancing slab pull

As an explanation to the fact that subducting slabs, although they are heated and weakened as they move through the mantle, do not bend to 90° dip angle, Jischke (Jischke, 1975) proposed that the slip zone (called hereafter channel) on top of the slab monotonically widens along depth, giving rise to underpressures that act normal to the slab surface against the slab pull (Fig. 1).

Let us define the pressure p (non-lithostatic pressure) as the difference of the actual pressure $P_{channel}$ within the channel to mantle lithostatic pressure at the same depth, i.e.

$$p = P_{channel} - \rho_m g z$$
 (all variables definitions are summarized in table 1). Overpressure

(underpressure) is defined as positive (negative) non-lithostatic pressure.

The slab pull force (Forsyth and Uyeda, 1975) depends on the density difference

$\Delta\rho_{mantle}$ between the subducting slab and surrounding mantle as

$$F_p = \Delta\rho_{mantle} gHL$$

where H and L are the slab thickness and length, respectively.

In the direction normal to the slab surface, the slab pull force F_p is equilibrated by the

traction pL resulting from the presence of underpressures within the channel

overlying the entire slab length, yielding:

$$p = \Delta\rho gH \cos \beta$$

where β is the dip angle.

Therefore, according to (Jischke, 1975) model, the amplitude of the underpressure is

controlled by the slab pull force. Density differences, arisen as the slab is colder than

surrounding mantle, are at most of the order of $100\text{kg}/\text{m}^3$ (Bina et al., 2001; Cloos,

1993; Jischke, 1975; Marton et al., 1999). Considering a slab with a thickness of

100km , a subduction dip of 45° , yields an estimate of average underpressure as

$$p \approx 70\text{MPa}$$

Such a value is clearly neglectible with respect to ambient mantle lithostatic pressure

and this model cannot account for large non-lithostatic pressures.

2.2 Balanced non-lithostatic pressure within the subduction channel

In (Jischke, 1975) model presented above, where the channel width is monotonically varying, underpressures are derived from the global force balance of the slab and are consequently bounded by the pull force exerted by the dense cold slab.

A alternative way to develop non-lithostatic pressure on top of the slab is to consider a confined flow of sediments within a rigid channel of varying width (Mancktelow, 1995).

In the precise configuration of (Mancktelow, 1995) model, the channel thins then widens, giving rise to overpressure upstream of the narrow point and underpressure downstream of it (Fig. 2). As overpressures are compensated by underpressures, their respective amplitude can grow arbitrarily large without much affecting the net force (i.e. summed over the slab surface), which still needs to be balanced by the slab pull force.

Then, within this subduction channel framework, even if instantaneous large non-lithostatic pressures can be potentially generated, a different question regards their persistence. Indeed, one can wonder whether non-lithostatic pressures, resulting from the non-uniformity of the channel width, would not tend to quickly deform the channel walls into parallelism and therefore annihilate themselves. A rapid examination of the correspondence between the topography and the non-lithostatic pressure (Fig. 2) shows that maxima of the non-lithostatic pressure coincide not with the extrema of channel topography but with the extrema of its gradient. Conversely, at points where the channel

is narrowest, the non-lithostatic pressure vanishes. Similarly, averaging the non-lithostatic pressure over a channel portion centered on the narrow point yields a null resulting force. As a result, if indeed non-lithostatic pressures act on the sections where width gradients are largest, they do not, or at least not in any simple fashion, tends to reduce the average gradient Δh . So non-lithostatic pressures presumably affect the channel geometry, but not necessarily in a self-destructing way.

The subduction channel of variable width described by (Mancktelow, 1995; Mancktelow, 2007) appears therefore as a reasonable candidate to generate large non-lithostatic pressure persistent over time-scales relevant for geological record.

3 Non-lithostatic pressure in the rigid subduction channel model

In this section we describe the subduction channel model and recall the results of (Mancktelow, 1995; Mancktelow, 2007) about the amplitude of non-lithostatic pressure in the case where the channel walls are not parallel and when the channel geometry is fixed, i.e. when the channel walls are sufficiently rigid so that they are not deformed.

3.1 General structure of the model

The subduction channel model (England and Holland, 1979; Shreve and Cloos, 1986) describes the circulation of crust on top of the subducting slab resulting from the concomitant action of the dragging by the subducting slab and the possible density

difference between crust and mantle (Raimbourg et al., 2007). The flow is laminar and confined within a channel bounded by the subducting lithospheric mantle below and the mantle wedge above (Fig. 3). The velocity of the crust is unidimensional and parallel to the slab. The crust within the channel can be seen as a thin layer as the width of the channel $h(x,t)$ is a few km, while its length L is of the order of 100's of km. As the mantle is considered as rigid with respect to the material within the channel, the channel walls do not deform and the geometry of the channel is fixed.

3.2 Constitutive equations

The flow within the channel is a Couette flow, i.e. a laminar flow of viscous material between two surfaces, for which the velocity field is given by (Batchelor, 1967):

$$u = \frac{\partial \phi}{\partial x} \frac{1}{2\mu_c} y(y-h) + U \left(1 - \frac{y}{h}\right) \quad (1)$$

Where μ_c is the crust viscosity, h the width of the channel, $0 \leq y \leq h$ the coordinate across the channel, $P_{channel}$ the pressure in the channel and

$\phi = P_{channel} - \rho_c g z$ the hydraulic potential. The non-lithostatic pressure p is defined as

before as the difference of the actual pressure $P_{channel}$ within the channel to mantle

lithostatic pressure at the same depth, i.e. $p = P_{channel} - \rho_m g z$. The gradient in hydraulic

potential can therefore be expressed as $\frac{\partial \phi}{\partial x} = \frac{\partial p}{\partial x} + g \sin \beta (\rho_m - \rho_c)$, where β is the

dip of the subduction.

The net flow through one section of the channel is equal to

$$Q = \int_0^h u dy = \frac{Uh}{2} - \frac{1}{\mu_c} \frac{\partial \phi}{\partial x} \frac{h^3}{12} \quad (2)$$

The mass conservation equations relate the flow gradient $\frac{\partial Q}{\partial x}$ to the time variations in

the channel width $\frac{\partial h}{\partial t}$ by

$$\frac{\partial Q}{\partial x} + \frac{\partial h}{\partial t} = 0 \quad (3)$$

As the channel geometry is fixed ($\frac{\partial h}{\partial t} = 0$), mass conservation equation (3) rewrites as

$$\frac{\partial Q}{\partial x} = \frac{U'}{2} \frac{\partial h}{\partial x} - \frac{\partial p}{\partial x} \frac{h^2}{4\mu_c} \frac{\partial h}{\partial x} - \frac{h^3}{12\mu_c} \frac{\partial^2 p}{\partial x^2} = 0 \quad (4)$$

where $\frac{U'}{2} = \frac{U}{2} - \frac{h^2}{4\mu_c} g \sin \beta (\rho_m - \rho_c)$

The term $\frac{U'}{2} \frac{\partial h}{\partial x}$ is a source term expressing the generation of non-lithostatic pressure

as the result of the interaction of a topography $\frac{\partial h}{\partial x}$ with a flow constituted of two

contributions: a flow resulting from dragging by the subducting slab ($\frac{U}{2}$) and a flow

resulting from density difference between crust and mantle ($\frac{h^2}{4\mu_c} g \sin \beta (\rho_m - \rho_c)$).

3.2 Non-lithostatic pressure amplitude in the rigid subduction channel

Considering the problem where the channel is monotonically narrowing then widening

(fig.2)

$$h = h_0 - \Delta h \frac{x}{L/2} \quad 0 \leq x \leq L/2$$

$$h = h_0 - \Delta h \left(2 - \frac{x}{L/2}\right) \quad L/2 \leq x \leq L$$

without density difference ($U' = U = cst$), the pressure field is given in (Batchelor,

1967) as

$$p = \frac{2\mu U}{L} \frac{6\Delta h x \left(\frac{L}{2} - x\right)}{\left(h - 2\Delta h \frac{x}{L}\right)^2 (2h - \Delta h)}$$

If the channel width variations are small. i.e. $\Delta h \ll h_0$, then

$$-\left(h - 2\Delta h \frac{x}{L}\right) \approx h_0$$

$$-(2h - \Delta h) \approx 2h_0$$

In such a simplified case, the pressure field can be therefore approximated as

$$p = \frac{2\mu U}{L} \frac{6\Delta h x \left(\frac{L}{2} - x\right)}{2h_0^3}$$

yielding as maximum pressure

$$p_{amp} = \frac{3}{8} \frac{\Delta h}{h_0} \frac{\mu U L}{h_0^2} \quad (5)$$

This simplified case clearly stresses the dependence of the non-lithostatic pressure on the various problem parameters.

First, the amplitude of non-lithostatic pressure is scaled by the viscosity of the material flowing within the channel: the larger its viscosity, the larger the non-lithostatic pressure within the channel. Second and maybe less intuitive is the dependence on the width of the channel: thinner channels strongly enhance the amplitude of non-lithostatic pressure.

For constant μ , U , L and relative thinning $\frac{\Delta h}{h_0}$, a channel constituted of 1-km

thick sediment pile develops non-lithostatic pressure 100 times larger than a channel

filled with a 10-thick crustal pile. This geometrical effect, known from the lubrication theory, is related to the strongly anisotropic shape ratio of the channel with $h_0 \ll L$.

4 Coupled model with deformation of the subduction channel walls

Following Eq. (5), arbitrarily large non-lithostatic pressure could be generated within the channel when considering arbitrarily viscous/thin crust. This is actually not correct, as Eq. (5) is only valid as long as the model assumptions are satisfied and in particular as long as the channel wall deformation can be neglected. For very viscous crust, the channel walls cannot longer be considered as rigid. Therefore, the amplitude the non-lithostatic pressure is in fact limited by the domain of validity of the model, which itself depends among other parameters on the ratio between the viscosity in the channel μ_c and the viscosity of the mantle, μ_m , which controls the deformation of the channel walls.

In his recent reappraisal of subduction channel dynamics, (Mancktelow, 2007) described numerical experiments including the deformation of the mantle bordering the channel.

His conclusion was that for the particular configuration used in the experiments, a ratio of $\frac{\mu_m}{\mu_c} \geq 10^7$ was a sufficient condition for the channel walls to be considered as rigid.

Similarly to this numerical approach, we develop in the following an analytical channel model that includes, in addition to the deformation within the channel, the deformation

of the channel walls. This coupled approach reflects the fact that variations in the non-lithostatic pressure within the channel may induce some deformation of the mantle surrounding it, therefore variations in the width of the channel, which in turn affect the pressure. This coupling seems of prime importance when crust viscosity becomes high, i.e. when non-lithostatic pressure is potentially large.

4.1 General structure of the model

In the case where deformation of the channel walls is considered, the term $\frac{\partial h}{\partial t}$ of the mass conservation equation (Eq. (3)) cannot be dropped and Eq. (3) is developed as

$$\frac{U'}{2} \frac{\partial h}{\partial x} - \frac{\partial p}{\partial x} \frac{h^2}{4\mu_c} \frac{\partial h}{\partial x} - \frac{h^3}{12\mu_c} \frac{\partial^2 p}{\partial x^2} + \frac{\partial h}{\partial t} = 0 \quad (6)$$

4.1.1 Deformation of mantle walls

The choice made in the previous equation of using not the total pressure $P_{channel}$ but rather the difference between $P_{channel}$ and the mantle lithostatic pressure P_m results from the fact that the latter P_m is the equilibrium pressure state for the mantle bordering the channel, and its actual state far from the subduction channel. Therefore, only the pressure difference defined as the non-lithostatic pressure p , triggers deformation of the mantle constituting the channel walls.

Additionally, due to temperature difference, the mantle within the slab is probably more rigid than its counterpart in the mantle wedge. Consequently, we assume in the

following that the basal boundary of the channel is flat and rigid, and that only the upper wall of the channel can deform when non-lithostatic pressure are generated. If the slab and the mantle wedge have similar viscosity, then the deformation of the channel walls is simply distributed between both foot and hanging walls, without much affecting the constitutive equations described hereafter.

The precise response of the mantle wedge to a non-lithostatic pressure field is complex and not precisely known, but we propose to use as approximate solution the deformation of a semi-infinite viscous media (mantle wedge) under the application of a load field (the non-lithostatic pressure p field in the channel) on its surface.

The deflection rate $\frac{dh}{dt}$ of the surface of a semi-infinite incompressible viscous medium of viscosity μ resulting from the application of a sinusoidal pressure field

$p = p_0 \sin \frac{2\pi}{l} x$ on its surface is given by (Biot, 1961) as

$$\frac{dh}{dt} = \frac{p_0 l}{4\pi\mu} \sin \frac{2\pi}{l} x = \frac{l}{4\pi\mu} p$$

If the actual non-lithostatic pressure field, which must satisfy $p=0$ for $x=0$ and $x=L$, is expressed as Fourier serie as

$$p = p_0 + \sum_{n=1}^{\infty} p_n^s \sin \frac{2\pi n}{L} x + \sum_{n=1}^{\infty} p_n^c \cos \frac{2\pi n}{L} x,$$

then, as the problem is linear, the resulting deflection is

$$\frac{dh}{dt} = \sum_{n=1}^{\infty} \frac{L}{4\pi n \mu} p_n^s \sin \frac{2\pi n}{L} x + \sum_{n=1}^{\infty} \frac{L}{4\pi n \mu} p_n^c \cos \frac{2\pi n}{L} x$$

i.e. the deformation generated in the mantle is inversely proportional to the frequency of the terms of the Fourier serie of the applied non-lithostatic field. Small wavelength terms (i.e. large n) result in mantle deformation whose amplitude is scaled by $\frac{1}{n}$, that is of limited amplitude.

In consequence of this wavelength dependence, no simple expression can be found to relate $\frac{dh}{dt}$ to any arbitrary pressure field p . Nevertheless, considering the actual pressure field resulting from the geometry depicted in Fig. 3 (with rigid channel wall assumption), which was also used in (Mancktelow, 1995), its form is relatively close to

$$p = p_0 \sin \frac{2\pi}{L} x$$

so that the amplitude of the higher terms of the serie is small. Similarly, even if the narrowing is concentrated in the central part of the channel, in the resulting pressure field the long wavelength term is still dominant (Fig. 3). Therefore, if the channel width is monotonically decreasing then increasing (or conversely) over L , whatever the precise channel topography, the pressure field can be broadly approximated by

$$p = p_0 \sin \frac{2\pi}{L} x$$

and the associated channel width variations by

$$\frac{dh}{dt} = \frac{L}{4\pi\mu_m} p \quad (7)$$

We consider in the following, as a first step of modeling, a channel with this schematic

geometry, i.e. a channel whose width variations have a lengthscale of the order of L , so that the channel width variations can be approximated by Eq. 7. We will show in section 6.3 that much shorter lengthscale variations can be reduced to this simple model.

4.1.2 Pressure-width coupled equations

Equations (6) and (7) control the coupled evolution of the pressure and channel geometry over time. Combining them gives

$$\frac{U'}{2} \frac{\partial h}{\partial x} - \frac{\partial p}{\partial x} \frac{h^2}{4\mu_c} \frac{\partial h}{\partial x} - \frac{h^3}{12\mu_c} \frac{\partial^2 p}{\partial x^2} + \frac{L}{4\pi\mu_m} p = 0 \quad (8)$$

(1) (2) (3)

which describes the instantaneous pressure field resulting from a given channel width profile.

4.2 Asymptotic behaviour of governing equation

Within the 3 pressure terms in Eq. 8 ((1), (2) and (3)), $\frac{\partial p}{\partial x} \frac{h^2}{4\mu_c} \frac{\partial h}{\partial x}$ and $\frac{h^3}{12\mu_c} \frac{\partial^2 p}{\partial x^2}$

(channel flow terms (1) and (2)) correspond to the response of the material flowing

within the channel to the channel geometry, while $\frac{L}{4\pi\mu_m} p$ (channel wall term (3))

corresponds to the channel wall deformation. Similarly to classical problems of flow in

boundary layers where the length L of the system is much larger than its width h

(e.g. the Prandtl boundary layer, e.g. (Elder and Williams, 1996)), we seek approximate

solutions to complete Eq. 8 by estimating the contribution of the different terms

composing it.

Consequently:

$$\text{Term (1): } \frac{\partial}{\partial x} \frac{h^2}{4\mu_c} \frac{\partial h}{\partial x} \approx \frac{1}{L^2} \frac{h_0^3}{4\mu_c}$$

$$\text{Term (2): } \frac{h^3}{12\mu_c} \frac{\partial^2 p}{\partial x^2} \approx \frac{1}{L^2} \frac{h_0^3}{12\mu_c}$$

The ratio of the channel flow terms ((1) or (2)) over the channel wall terms (3) is

therefore approximately given by the adimensional factor

$$\alpha = \frac{\mu_m}{\mu_c} \frac{h_0^3}{L^3}$$

The behaviour of Eq. 8 depends on the value of α , and in particular in the domains

where $\alpha \ll 1$ and $\alpha \gg 1$, some of its terms, either (3) or (1) and (2), respectively, get

neglectible, so that Eq. 8 can be simplified into asymptotic forms.

- "high α " endmember regime

For $\alpha \gg 1$, equation (8) can be simplified as

$$\frac{U'}{2} \frac{\partial h}{\partial x} - \frac{\partial p}{\partial x} \frac{h^2}{4\mu_c} \frac{\partial h}{\partial x} - \frac{h^3}{12\mu_c} \frac{\partial^2 p}{\partial x^2} = 0 \quad (9.1)$$

This "high α " regime is the "classical" one, where the geometry of the channel is fixed

as a result of high mantle viscosity, which prevents channel walls deformation. The flux

is constant throughout the channel.

- "low α " endmember regime

For $\alpha \ll 1$, equation (8) reduces to

$$\frac{U'}{2} \frac{\partial h}{\partial x} + \frac{L}{4\pi\mu_m} p = 0 \quad (9.2)$$

This "low α " regime is diametrically different from the "classical" model described hereafter, as the geometry of the channel evolves over time, therefore the flux varies in time and space. In this regime, the pressure is controlled by the deformation of the channel walls, which is enabled by the "low" viscosity of the mantle.

4.3 Amplitude of non-lithostatic pressure

4.3.1 Particular geometry

As an illustration of the problem, we consider in this section the numerical solution to complete Eq. (6) for a channel whose initial topography profile is given by (Fig. 4):

$$h = h_0(0.9 + 0.1\cos(\frac{2\pi x}{L})) \quad 0 \leq x \leq L \quad (10)$$

i.e. channel narrowing then widening back over a length L . We do not aim here at analyzing the time-evolution of the channel geometry, but rather to take an instantaneous picture of the channel state for a given topography and in particular to estimate the amplitude of overpressure, defined as

$$p_{amp} = \max(|p(x)|) \quad 0 \leq x \leq L$$

4.3.2 Asymptotic solutions

Regardless of their relevance to the complete Eq. 8, simplified equations (9.1) and (9.2) can be approximately solved for this particular system geometry.

- "high α " endmember regime

As the variations of U' along the channel for the particular geometry given by (10) are small ($\frac{\Delta U'}{U'} \approx \frac{\Delta h}{h} \approx 0.1$), they can be neglected in order to obtain a approximate but simpler solution, computed as

$$\frac{\partial p}{\partial x} \approx \frac{\mu_c U'}{h_0^2} \frac{1}{(0.9 + 0.1 \cos \frac{2\pi x}{L})^3} (0.1 - 0.6 \cos \frac{2\pi x}{L}) \quad 0 \leq x \leq L$$

yielding

$$p_{amp}^{high \alpha} \approx 0.13 \frac{\mu_c U' L}{h_0^2} \quad (11.1)$$

which is very similar to the rigid channel approximate solution Eq. 5. The dependence on the channel thickness is once again apparent and thin channel develop strongly amplified non-lithostatic pressure.

- "Low α " endmember regime

Under the same assumption that $U' \approx cst$, Eq. 9.2 can solved to obtain the amplitude of non-lithostatic pressure as

$$p_{amp}^{low \alpha} = 4\pi^2 \Delta h \frac{U'}{L^2} \mu_m, \text{ yielding}$$

$$p_{amp}^{low \alpha} \approx 39.5 \frac{U' \Delta h}{L^2} \mu_m \quad (11.2)$$

4.3.3 Maximum non-lithostatic pressure controlled by the channel wall deformation

We solved numerically Eq. 8 for the channel geometry given by Eq. 10 and given values of all the parameters. As graphical representation, by analogy with similar studies (Mancktelow, 1995; Mancktelow, 2007), we plotted p_{amp} as a function of increasing

μ_c , all the other parameters being kept constant (Fig. 5). Nevertheless, in order to highlight the role of $\alpha = \frac{\mu_m h_0^3}{\mu_c l^3}$, which controls the equation behaviour, in Fig. 5 we

used as abscissa not simply the crust viscosity, μ_c , but crust viscosity multiplied by a constant factor, $\frac{1}{\mu_m} \frac{L^3}{h_0^3}$, as the product is equal to the inverse of α ($\mu_c \frac{1}{\mu_m} \frac{l^3}{h_0^3} = \frac{1}{\alpha}$).

The numerical solution rapidly converges towards the two asymptotic solutions outside of the central domain where $\alpha \approx 1$. Furthermore, the non-lithostatic pressure amplitude is always bounded by the lower of the two asymptotic solutions. As the crust viscosity μ_c increases from very low values (corresponding to high- α domain), the amplitude of the non-lithostatic pressure increases at the same rate as high- α endmember solution (Eq. 11.1), the solution for a rigid channel. Then as μ_c gets larger (i.e. in the domain $\alpha \approx 1$), the deformation of the channel wall cannot be disregarded anymore and the actual non-lithostatic pressure, although still increasing, diverges from high- α endmember solution. Finally, as μ_c get so large that $\alpha \ll 1$, the amplitude of non-lithostatic pressure, always increasing but at a slower and slower rate, converge asymptotically towards the low- α endmember solution (Eq. 11.2), i.e. towards the case where the pressure within the channel is controlled by the deformation of the channel walls. This conclusion should not be misunderstood: we did not show that the non-lithostatic pressure disappears quickly due to mantle deformation; but that the

deformation of the channel wall *instantly* prevents arbitrarily large non-lithostatic pressure to exist within the channel.

The largest non-lithostatic pressure over the parameter space that possibly develops within the channel is bounded by the solution to the simplified low- α equations. From the solution to a particular channel configuration given by Eq. 11.2, a generic form of the largest non-lithostatic pressure (called hereafter p_{\max}) can be expressed as:

$$p_{\max} = f(\text{geom}) \frac{U' \Delta h}{L^2} \mu_m \quad (12)$$

where $f(\text{geom})$ is a numerical factor that depends on the precise geometry of the subduction channel. As apparent in Eq. 12, the maximal amplitude of the non-lithostatic pressure is independent on μ_c , i.e. independent on the properties of the material flowing within the channel. Material within the channel controls to which extent the actual flow regime is close to this limit, but the limit itself is control only by the mantle constituting the channel.

6 Discussion

6.1 Maximum non-lithostatic pressure in subduction zones

6.1.1 Application of coupled channel approach to existing problems

In his pioneering approach of overpressures in subduction zones, (Mancktelow, 1995)'s study considers a channel filled with sediments bounded by mantle infinitely rigid. The

parameters are as follows:

$$h_{average} = 10^3 m = h_0 \quad , \quad \Delta h = h_{max} - h_{min} = 900 m \quad , \quad L = 250 km \quad , \quad \mu_s = 6.10^{18} Pa.s \quad ,$$

$$U = 8cm / yr$$

blueschist sediments density: $\rho_s = 3250 kg.m^{-3}$

asthenospheric density: $\rho_m = 3350 kg.m^{-3}$

$$U \approx \frac{h^2}{2\mu_s} g(\rho_m - \rho_s) \Rightarrow U' \approx U$$

Although in (Mancktelow, 1995)'s assumptions, mantle has infinite viscosity ($\mu_m = \infty$),

we can try to assign realistic values to μ_m , and use for the rest of parameters the same

values as his, and estimate what the coupled channel approach used here would predict.

Calculating the value of $\alpha = \frac{\mu_m}{\mu_c} \frac{h_0^3}{L^3}$ for this set of parameters gives

$$\mu_m = 10^{23} Pa.s \rightarrow \alpha = 1.07 \cdot 10^{-3}$$

$$\mu_m = 10^{25} Pa.s \rightarrow \alpha = 1.07 \cdot 10^{-1}$$

therefore $\alpha \ll 1$. Accordingly, for these values of mantle viscosity, even if the mantle is

still much stronger than sediments, the channel wall deformation cannot be neglected

and resulting non-lithostatic pressure is lower than calculated with the rigid channel

assumptions.

This estimation points the importance of the geometry in addition to viscosity contrast

to determine whether the channel is rigid or not. α depends of course on the viscosity

ratio $\frac{\mu_m}{\mu_c}$ but also on the geometry of the channel through the factor $\frac{h_0^3}{L^3}$, of the order of 10^{-7} in this particular case.

This effect of geometry is apparent in the 2-D numerical model of (Mancktelow, 2007), in which the deformation of the channel walls is explicitly considered. For $\mu_c \leq 10^{-7} \mu_m$, the rigid-wall assumption is effectively met, while when μ_c is increased in the range $10^{-7} \mu_m \leq \mu_c \leq \mu_m$, the non-lithostatic pressure within the channel deviates more and more from the rigid-channel solution. From his figure 17b, the deviations can be considered as significant from $\mu_c \geq 10^{-5} \mu_m$. In (Mancktelow, 2007)'s geometry,

$\frac{h_0}{L} = \frac{1}{64}$ (his channel length is half what we defined as channel length), yielding for

$$\mu_c = 10^{-5} \mu_m :$$

$$\alpha = \frac{\mu_m}{\mu_c} \frac{h_0^3}{L^3} \approx 0.38$$

in agreement with the condition $\alpha \approx 1$ for the limit of applicability of rigid channel model.

6.1.2 Estimates of maximum non-lithostatic pressure

Using the material parameters of (Mancktelow, 1995), we can estimate the maximum overpressure in the channel, using Eq. 11.2 as approximate solution, yielding

$$p_{\max} = 1.56 \cdot 10^{-15} \mu_m$$

Therefore, for $\mu_m = 10^{23} Pa.s$, $p_{\max} = 156 MPa$ and for $\mu_m = 10^{24} Pa.s$, $p_{\max} = 1.56 GPa$. These values, very similar to (Mancktelow, 2007)'s estimates based on numerical simulations, are upper bounds on the actual pressures within the channel. Our coupled model developed here shows that rather than the viscosity of the crust within the channel, the largest control on the actual non-lithostatic pressure within the channel lies in the properties of the mantle within the slab and the mantle wedge. If either one of the two is relatively hot and deformable, with μ_m of the order of $10^{23} Pa.s$, then non-lithostatic pressure is necessarily of limited amplitude. On the contrary, in the configuration where both mantle wedge and slabs are cold and very viscous, non-lithostatic pressure can grow very large, up to the order of ambient lithostatic pressure.

6.2 Control of channel geometry on the amplitude of actual non-lithostatic pressure

6.2.1 Non-lithostatic pressure dependence on channel thickness

The direct influence of the channel width h_0 on the non-lithostatic pressure amplitude is apparent in Eq. 5 and 11.1: for constant μ_c , μ_m , U , L and width variations Δh , non-lithostatic pressure amplitude varies as $\frac{1}{h_0^3}$, i.e. is much increased in thin channels, which is a classical result of lubrication theory.

On the other hand, an increase in the channel non-lithostatic pressure amplitude results in larger deformation of the channel walls, which reduces this increase. This “regulation” process is apparent through the variations of the parameter α , which is proportional to h_0^3 (Fig. 6): considering two channels of width h_0 and $\frac{h_0}{10}$, the rigid channel solution predicts non-lithostatic pressure amplitude larger by a factor 1000 for the latter crust (Δp^{rig}). But as, for a given μ_c , α is much lower for the $\frac{h_0}{10}$ crust, it deviates much more from the rigid channel solution, yielding a smaller actual pressure difference between the two channels ($\Delta p^{cpd} < \Delta p^{rig}$). Considering coupled equations tends therefore to reduce the effect of channel thickness on non-lithostatic pressure amplitude. Eventually, i.e. for large μ_c , the difference between the two channels vanishes, as the maximum non-lithostatic pressure does depend neither on the crust thickness nor on its viscosity, so that they both converge towards the same asymptotic limit.

6.2.1 Non-lithostatic pressure dependence on the lengthscale of channel topography

The simple geometries used here or in (Mancktelow, 1995; Mancktelow, 2007) enable to derive simple solutions to the narrowing channel problem. Nevertheless, real channel geometry is likely to be different, and its characteristics possibly bear some influence on the distribution of the non-lithostatic pressure arisen. In particular, we have supposed, to

describe the deformation of the channel walls (Eq. 7), that the lengthscale of the perturbations of the channel width were of the order of channel length, i.e. 100's of km. Although perturbations related to slab bending have probably a long lengthscale, those related to serpentinization of the mantle wedge or to subducting seamounts are probably of much shorter lengthscale.

The pressure field resulting from channel perturbation whose lengthscale is reduced from L to $L' = \frac{L}{10}$ can be easily obtained from the repetition of the solution we have found for a single channel narrowing (Eq. 11.1), using L' instead of L .

As a result, the parameter α is increased by a factor equal to $\frac{\alpha^{L'}}{\alpha^L} = \left(\frac{L}{L'}\right)^3 = 10^3$, i.e. for constant material properties μ_c and μ_m , the channel behaves much more rigidly.

Consequently, as explained in 6.1, even for the same values of viscosities and channel wall convergence angle ($\frac{\Delta h}{L} = \frac{\Delta h'}{L'}$), the non-lithostatic pressure reaches higher amplitude.

The explanation for this phenomenon lies in the response of the mantle to the applied non-lithostatic pressure field, which is scaled by the lengthscale of the pressure field variations (see section 4.1.1). As a result, the deformation of the channel walls, for the same pressure amplitude, is strongly reduced for a pressure field with shorter lengthscale:

$$\left. \frac{dh}{dt} \right)_{L=\frac{L}{10}} = \frac{L}{4\pi\mu_m} p = \frac{1}{10} \frac{L}{4\pi\mu_m} p = \frac{1}{10} \left. \frac{dh}{dt} \right)_L$$

i.e. channel deformation rate is reduced by a factor 10 when the lengthscale of the channel pressure field is divided by 10.

In summary, the mantle deforms more easily if the pressure gradient is applied over a larger distance. Small-scale perturbations of the channel width trigger the development of non-lithostatic pressure field with larger amplitude.

7 Conclusions:

Our approach coupling both deformation of the crust within the channel and the mantle bounding it shows that maximum non-lithostatic pressure within the channel is controlled by the properties of the mantle, irrespectively of the nature of the subducting crust. The deformation of the walls of the channel, resulting from the existence of non-lithostatic pressure within the channel, instantly prevents arbitrarily large non-lithostatic pressure to develop. The transition from the rigid channel model to a regime where the deformation of the channel walls controls the non-lithostatic pressure amplitude within the channel is controlled by the adimensional parameter α , which includes both the viscosity ratio as well as the geometry of the system.

References

- Batchelor, G.K., 1967. An introduction to fluid dynamics, Cambridge University Press, New York.
- Bina, C.R., Stein, S., Marton, F.C., Van Ark, E.M., 2001. Implications of slab mineralogy for subduction dynamics. *Phys. Earth Planet. In.* 127, 51-66.
- Biot, M.A., 1961. Theory of folding of stratified viscoelastic media and its implication in tectonics and orogenesis. *Geol. Soc. Am. Bull.* 72, 1595-1620.
- Burg, J.-P., Gerya, T.V., 2005. The role of viscous heating in Barrovian metamorphism of collisional orogens: thermomechanical models and application to the Lepontine Dome in the Central Alps. *J. Metamorph. Geol.* 23, 75-95.
- Burov, E., Jolivet, L., Le Pourhiet, L., Poliakov, A., 2001. A thermomechanical model of exhumation of high pressure (HP) and ultra-high pressure (UHP) metamorphic rocks in Alpine-type collision belts. *Tectonophysics* 342, 113-136.
- Chopin, C., 1984. Coesite and pure pyrope in high-grade blueschists of the western Alps: A first record and some consequences. *Contrib. Mineral. Petrol.* 86, 107-118.
- Cloos, M., 1993. Lithospheric buoyancy and collisional orogenesis: Subduction of oceanic plateaus, continental margins, island arcs, spreading ridges and seamounts. *Geol. Soc. Am. Bull.* 105, 715-737.
- Duchêne, S., Ford, M., 2006. Exhumation of the Dora Maira UHP unit: a special case? *Geophys. Res. Abs.* 8, 03500.
- Elder, S.A., Williams, J., 1996. Fluid physics for oceanographers and physicists, Butterworth-Heinemann, Oxford.
- England, P.C., Holland, T.J.B., 1979. Archimedes and the Tauern eclogites: the role of buoyancy in the preservation of exotic eclogite blocks. *Earth Planet. Sci. Lett.* 44, 287-294.
- Forsyth, D.W., Uyeda, S., 1975. On the relative importance of driving forces on plate motion. *Geophys. J. R. Astr. Soc.* 43, 163-200.
- Gerya, T.V., Stöckhert, B., Perchuk, A.L., 2002. Exhumation of high-pressure metamorphic rocks in a subduction channel: a numerical simulation. *Tectonics* 21, doi:10.1029/2002TC001406.
- Guillot, S., Hattori, K.H., De Sigoyer, J., 2000. Mantle wedge serpentinization and eclogite exhumation: Insight from eastern Ladakh, northwest Himalaya. *Geology* 28,

199-202.

- Guillot, S., Hattori, K.H., de Sigoyer, J., Nagler, K., Auzende, A.-L., 2001. Evidence of hydration of the mantle wedge and its role in the exhumation of eclogites. *Earth Planet. Sci. Lett.* 193, 115-127.
- Houseman, G.A., Gubbins, D., 1997. Deformation of subducted oceanic lithosphere. *Geophys. J. Int.* 131, 535-551.
- Jischke, M.C., 1975. On the dynamics of descending lithospheric plates and slip zones. *J. Geophys. Res.* 80, 4809-4813.
- Mancktelow, N.S., 1993. Tectonic overpressure in competent mafic layers and the development of isolated eclogites. *J. Metamorph. Geol.* 11, 801-812.
- Mancktelow, N.S., 1995. Nonlithostatic pressure during sediment subduction and the development and exhumation of high pressure metamorphic rocks. *J. Geophys. Res.* 100, 571-583.
- Mancktelow, N.S., 2007. Tectonic pressure: Theoretical concepts and modelled examples. *Lithos* in press.
- Marton, F.C., Bina, C.R., Stein, S., 1999. Effects of slab mineralogy on subduction rates. *Geophys. Res. Lett.* 26, 119-122.
- Petrini, K., Podladchikov, Y., 2000. Lithospheric pressure-depth relationship in compressive regions of thickened crust. *J. Metamorph. Geol.* 18, 67-77.
- Pilchin, A., 2005. The role of serpentinization in exhumation of high- to ultra-high-pressure metamorphic rocks. *Earth Planet. Sci. Lett.* 237, 815-828.
- Raimbourg, H., Jolivet, L., Leroy, Y., 2007. Consequences of progressive eclogitisation on crustal exhumation, a mechanical study. *Geophys. J. Int.* 168, 379-401.
- Shreve, R.L., Cloos, M., 1986. Dynamics of sediment subduction, melange formation, and prism accretion. *J. Geophys. Res.* 91, 10229-10245.
- Smith, D.C., 1984. Coesite in clinopyroxene in the Caledonides and its implications for geodynamics. *Nature* 310, 641-644.
- Stuwe, K., Sandiford, M., 1994. Contribution of deviatoric stress to metamorphic P-T paths: an example appropriate to low-P, high-T metamorphism. *J. Metamorph. Geol.* 12, 445-454.
- Toussaint, G., Burov, E., Avouac, J.-P., 2004. Tectonic evolution of a continental collision zone: a thermomechanical numerical model. *Tectonics* 23, doi:10.1029/2003TC001604.

Figure captions

Figure 1: Development of non-lithostatic pressure within the subduction channel as a result of channel monotonic widening, following the model by Jischke (Jischke, 1975).

(A) the subduction channel act as a lubricating layer ((Batchelor, 1967)-p219) at the interface of the two plates. (B) As a result of channel widening between h_0 and $h_0 + \Delta h$, the pressure $P_{channel}$ within the channel is slightly lower than the pressure P_m of the mantle at the same depth. (C) The resulting underpressure p ($p = P_m - P_{channel}$) exerts a force on the slab equilibrating the slab pull force F_p . The curves were calculated without taking into account the density difference between channel and mantle, and assuming channel widening by a factor 2, i.e. $\Delta h = h_0$.

Figure 2: Development of non-lithostatic pressure in a subduction channel that narrows then widens back to its original width. The pressure profile is antisymmetric, with overpressure in the narrowing portion and underpressure in the widening portion of the channel, so that the net force exerted on the slab is null. The curves were calculated without taking into account the density difference between channel and mantle, and

assuming channel narrowing such that $\Delta h = \frac{3h_0}{4}$.

Figure 3: The subduction channel model used here describes the circulation of the crust overlying the subducting slab. In our model width $h(x)$ and pressure $P(x)$ are coupled: spatial variations in the width of the channel result in the formation of a non-lithostatic pressure ($p = P_{channel} - \rho_m g z$) that affects the flow pattern (A), but which also triggers the deformation of mantle bounding the channel, which in turn controls the time variations of $\frac{\partial h(x)}{\partial x}$ (B).

Figure 4: Pressure field calculated for the given sinusoidal profile of $h(x)$ in the two extreme regimes $\alpha \ll 1$ and $\alpha \gg 1$. The profiles have similar shapes, in particular overpressures within the narrowing section of the channel are compensated by underpressures in the widening section. In contrast, the amplitude of the non-lithostatic pressure p_{amp} is variable (the profiles are not scaled with respect to each other).

Figure 5: Evolution of the dimensional non-lithostatic pressure amplitude p_{amp} for increasing μ_c . The variable μ_c in abscissa is scaled by $\frac{L^3}{\mu_m h_0^3}$, which is kept constant. As a consequence, for large μ_c , α is low and p_{amp} converges towards the “low α ” solution. Conversely, for low μ_c , α is large and p_{amp} converges towards the “high α ”, i.e. the rigid channel, solution. Maximum non-lithostatic pressure is reached in the domain $\alpha \ll 1$, i.e. where the pressure field is controlled by the channel wall

deformation. The upper bound on p_{amp} is equal to $p_{amp}^{low\alpha} = 4\pi^2 \Delta h \frac{U'}{L^2} \mu_m$.

Figure 6: Schematic evolution of non-lithostatic pressure amplitude p_{amp} for increasing crustal viscosity (without log-scale, in contrast with Fig.5). For low μ_c , the deformation of the channel walls is neglectible, and p_{amp} increases in proportion of μ_c increase. When μ_c gets larger, the flow of crust within the channel trigger channel wall deformation, so that actual increase in p_{amp} deviates from linear increase (dashed curves) and asymptotically converge to $p_{amp}^{max} = f(geom) \frac{U' \Delta h}{L^2} \mu_m$, which does not depend on μ_c as it is controlled only by channel walls deformation. The transition from “No channel wall deformation” to “Deformation of channel walls” corresponds to the transition from $\alpha \ll 1$ to $\alpha \approx 1$. The rigid channel solution predicts that a channel of width $\frac{h_0}{10}$ is affected by non-lithostatic pressure amplified by a constant factor with respect to a channel of width h_0 . As, for given μ_c , α is also much decreased for a thinner crust, the actual non-lithostatic pressure difference between the two channel geometry, Δp^{cpd} , is smaller than the difference Δp^{cpd} predicted in the rigid channel model. For large μ_c , the pressure for both geometries converge towards the same limit and the geometrical effect vanishes.

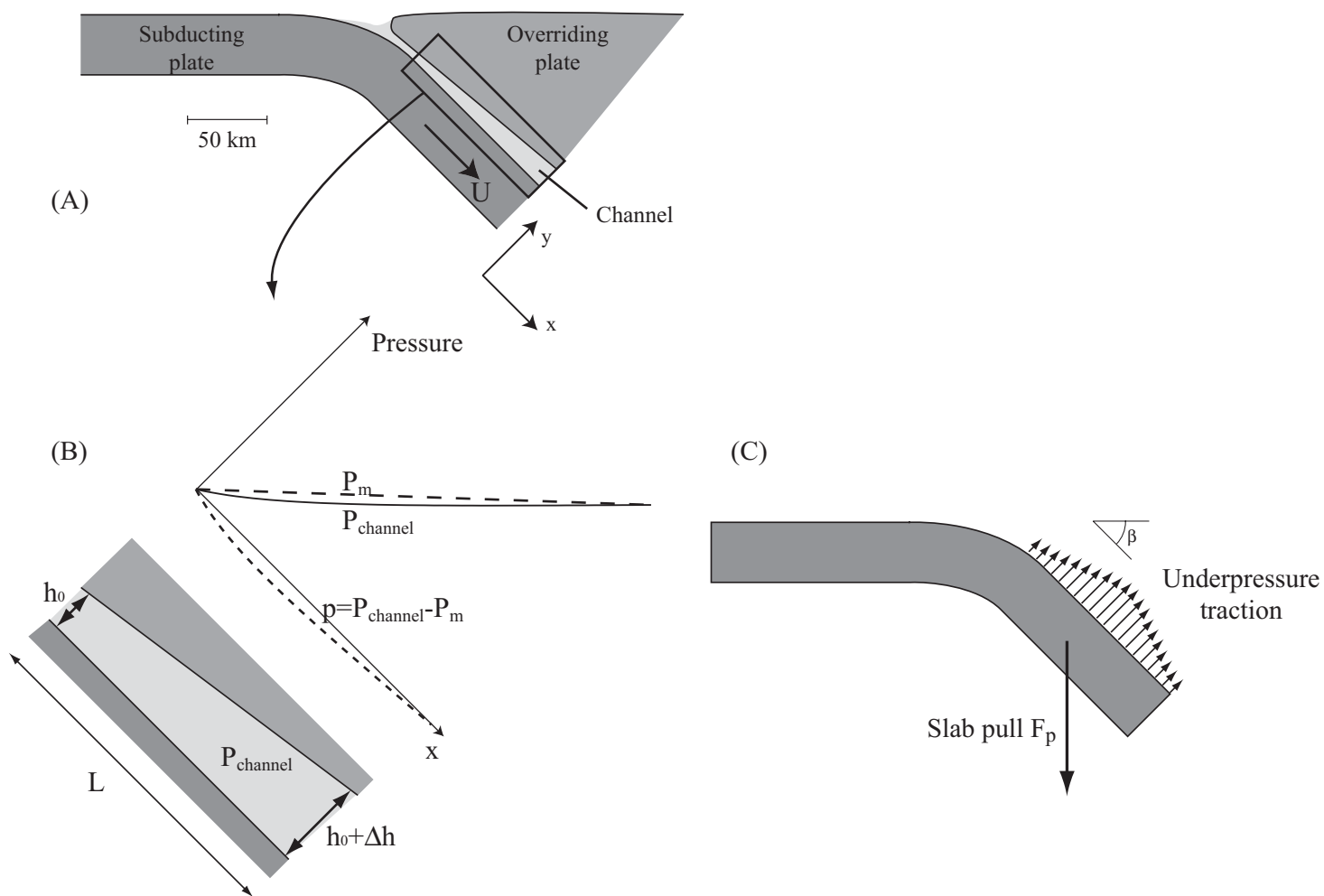


Fig
1

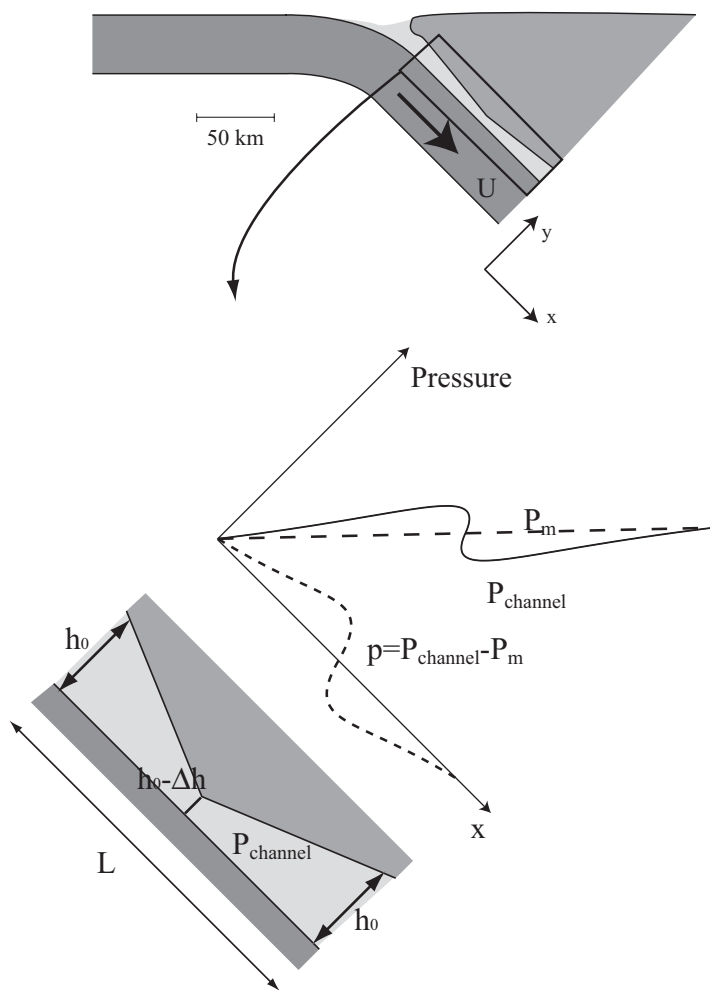


Fig
2

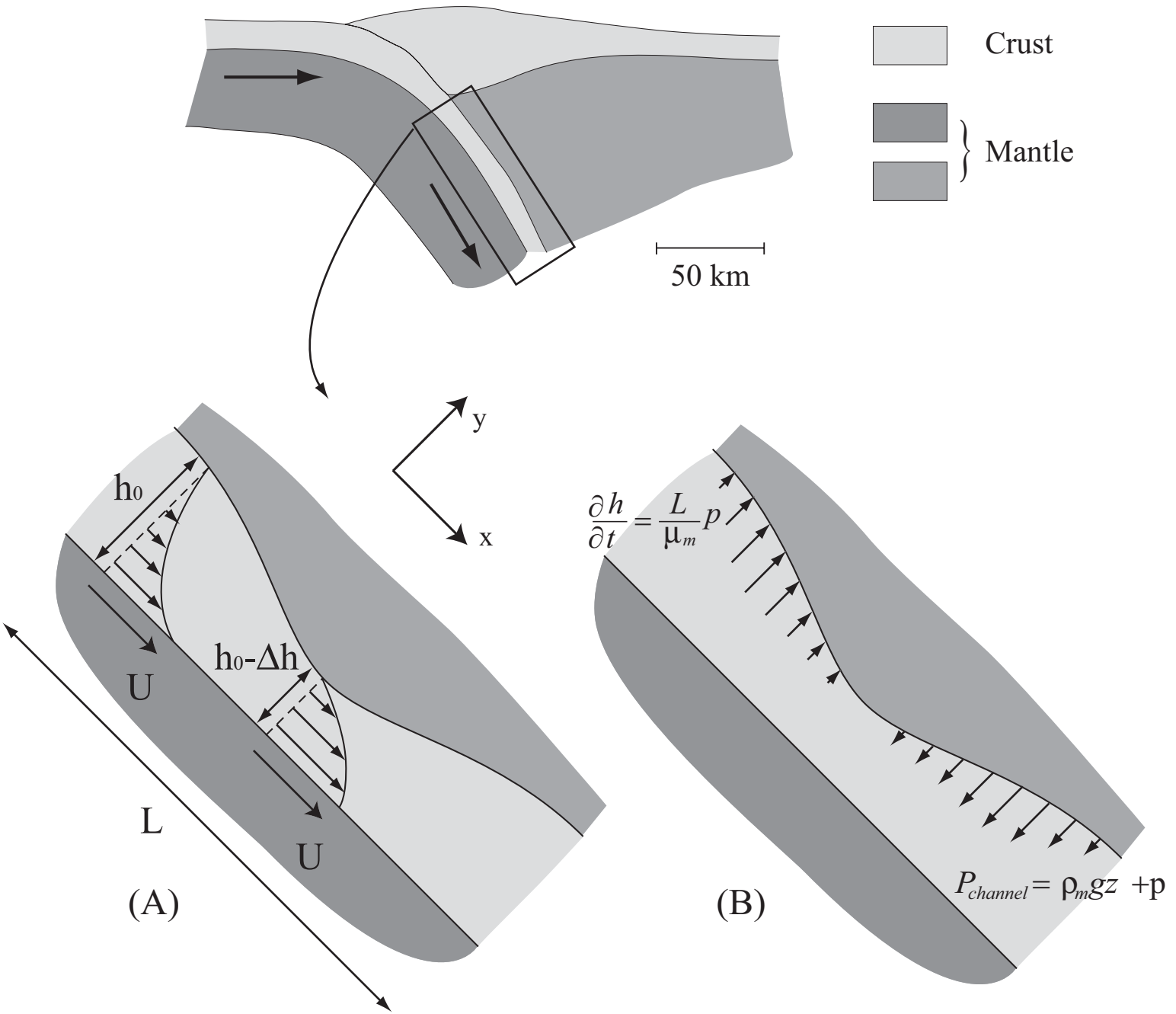


Fig
3

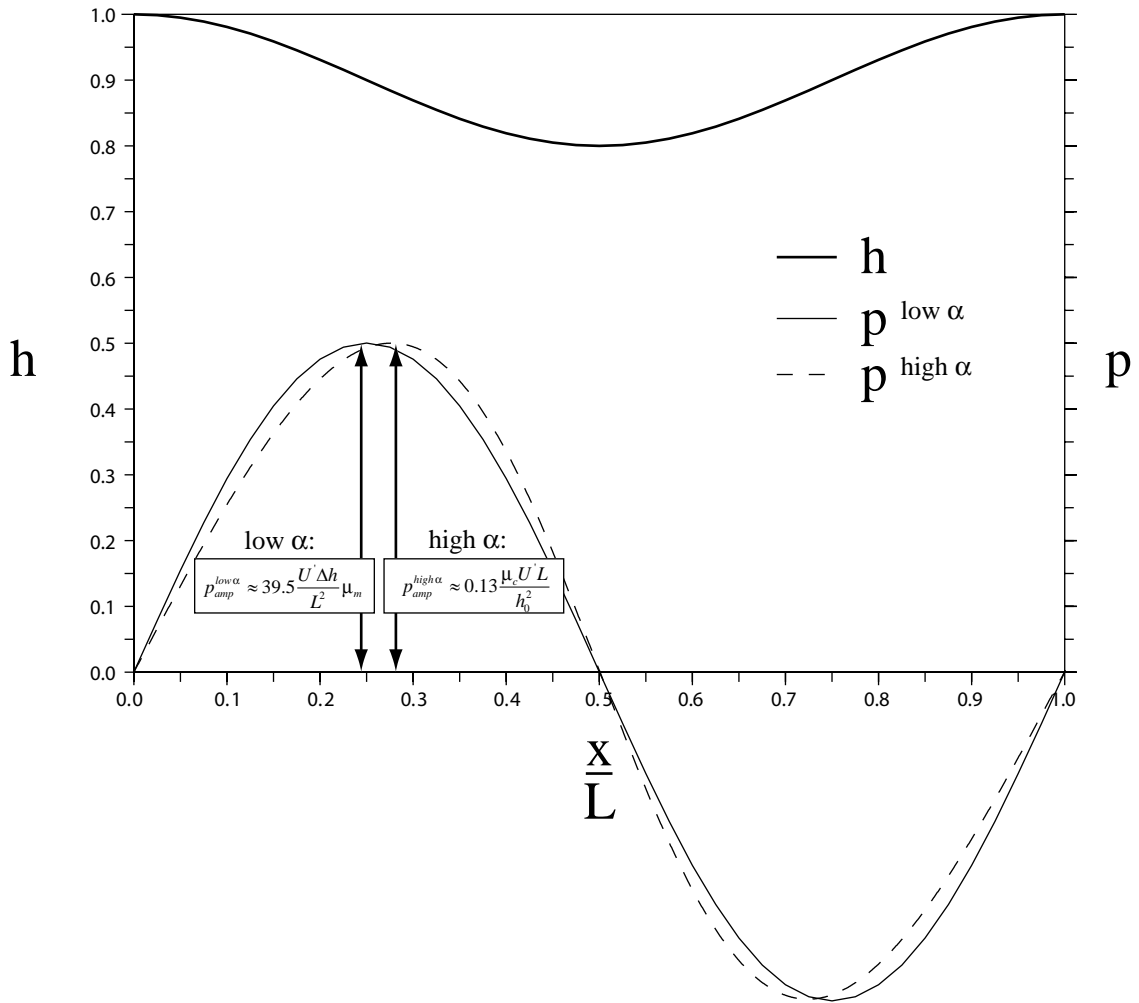


Fig
4

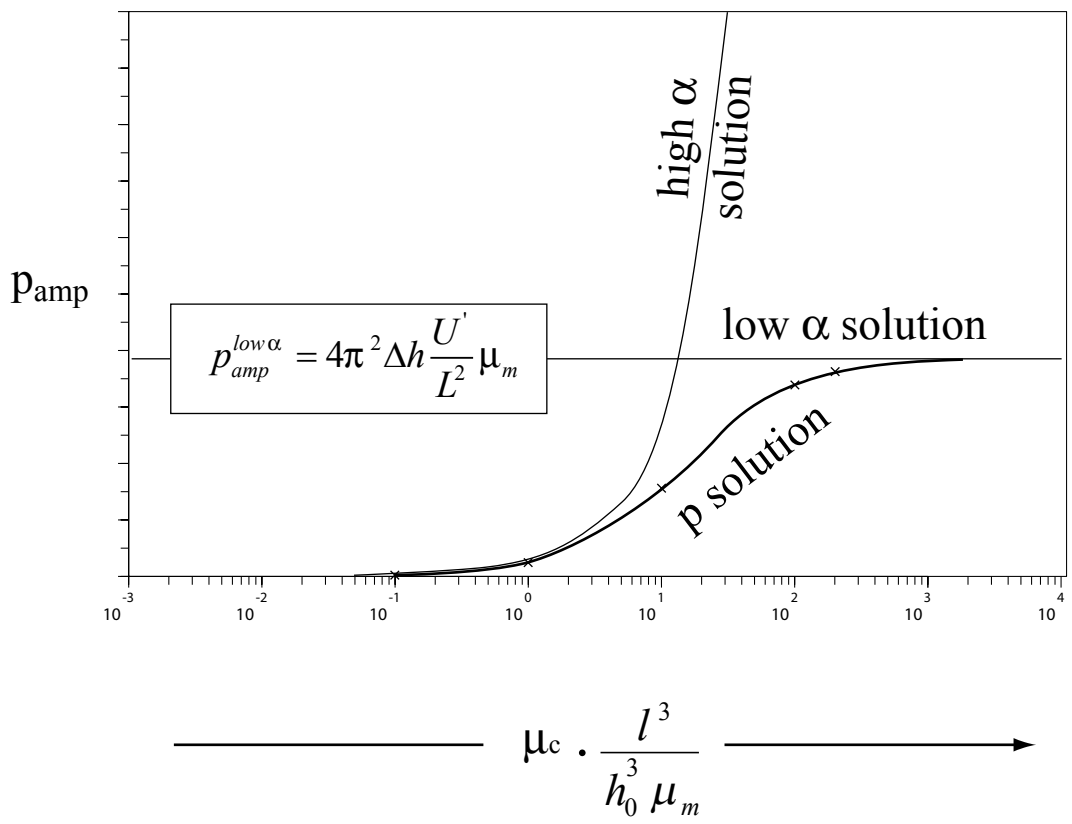


Fig 5

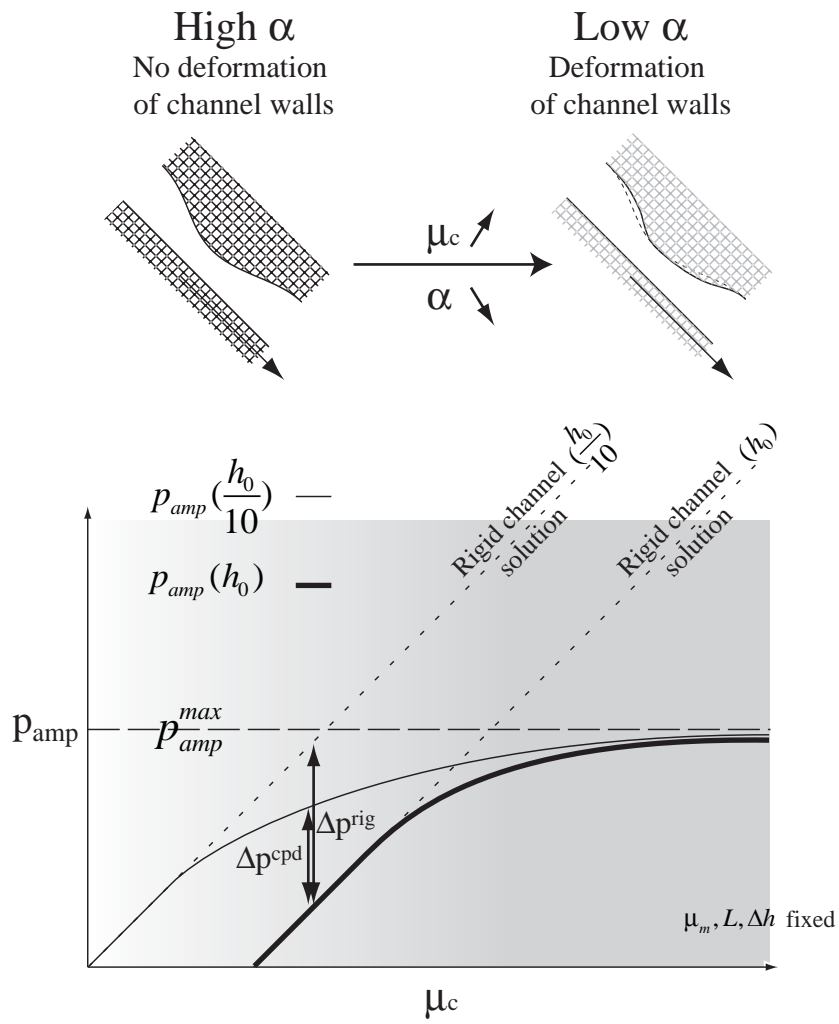


Fig
6